A Single-Chamber Pneumatic Soft Bending Actuator With Increased Stroke-Range by Local Electric Guidance

Meng Luo, Lei Liu, Chen Liu, Bo Li, *Member, IEEE*, Chongjing Cao, Xing Gao, and Dichen Li

***Abstract*—Thanks to their continuously deformable features, soft bending actuators, including pneumatic and electric actuators, are increasingly used in continuum robots. Further development, however, is limited by the complexity of the multicavity structure in pneumatic actuators and the instability of the electromechanical coupling in dielectric elastomer actuators. In this article, by combining the advantages of the two actuation techniques, a novel hybrid electro-pneumatic bending actuator is proposed that is capable of bending with significantly reduced complexity and improved stability. A timing control method is proposed that enables rapid and significant bending. A low voltage is used for bending guidance with air-pressure concurrently to produce a large bending stroke. The results of experiments indicate that, with increasing air pressure, the bending angle varies in three different stages. These stages are (I) a low-pressure guidance stage, (II) an instability induction stage, and (III) a stable deformation stage. By harnessing the instability at stage II, the driving voltage can be substantially reduced to avoid electric breakdown. By studying the effect of prestretch on bending, the controllability of the bending deformation is improved. The simulation is also used to verify the control method and predict the development path of soft robots.**

***Index Terms*—Control design, electro-pneumatic actuators, numerical simulation, soft robotics.**

Manuscript received March 2, 2020; revised June 3, 2020; accepted July 8, 2020. Date of publication August 6, 2020; date of current version June 16, 2021. This work was supported in part by the National Natural Science Foundation of China under Grant 51805413 and Grant 91748124, in part by the National Key R&D Program of China under Grant 2019YFB1311600, and in part by the Shaanxi Key Research and Development Program under Grant 2020ZDLGY06-11. *(Meng Luo and Lei Liu contributed equally to this work.) (Corresponding authors: Bo Li; Dichen Li.)*

Meng Luo, Chen Liu, Bo Li, and Dichen Li are with the State Key Laboratory for Manufacturing System Engineering, School of Mechanical Engineering, Xi'an Jiaotong University, Xi'an 710049, China (e-mail: 1378295806@qq.com; gtlchen@stu.xjtu.edu.cn; liboxjtu@xjtu.edu.cn; dcli@xjtu.edu.cn).

Lei Liu is with the School of Mechanical and Precision Instrument Engineering, Xi'an University of Technology, Xi'an 710048, China (e-mail: liulei@xaut.edu.cn).

Chongjing Cao and Xing Gao are with the Research Centre for Medical Robotics and Minimally Invasive Surgical Devices, Shenzhen Institutes of Advanced Technology,Chinese Academy of Sciences, Shenzhen 518055, China (e-mail: cj.cao@siat.ac.cn; xing.gao@siat.ac.cn).

Color versions of one or more of the figures in this article are available online at https://ieeexplore.ieee.org.

Digital Object Identifier 10.1109/TIE.2020.3013544

I. Introduction

SOFT robots have evolved rapidly in recent years, with a wide range of applications that emerged in the fields of material research, stretchable sensors, and mechanical design [1]–[5]. A soft robot can produce continuous deformation and shows environmental adaptability—especially in extreme environments. It is regarded as a cutting-edge technology that outperforms conventional multijoint robots. Some bio-inspired designs and material modifications are utilized to manufacture soft robots that feature a variety of motion modes such as wall climbing [6], underwater flapping wings [7], air flight [8], and jet motion [9].

Soft actuators, in particular, those that have multiple degrees of freedom, play an essential role in the development of soft robots. For example, in the soft pneumatic actuator, with a combination of chamber inflation, a sophisticated 3-D motion is achieved [10]. As shown in Fig. 1, the current actuation methods of soft robots are very different from the conventional multijoint hinged mechanism in a continuum robot for engine repair [11] [see Fig. 1(a)]. They tend to use materials that allow continuous deformation, which is enabled by pneumatic pumping [12] [see Fig. 1(b)] or electric actuation in the electroactive polymers in the roll-up configuration [13] [see Fig. 1(c)]. The advantages of pure pneumatic actuation are improved convenience, thanks to a simplified control method. On the other hand, there are also disadvantages, such as the complicated pneumatic chambers inside the robot body [14]–[16], and a pumping system for pressure support. However, thanks to the use of electroactive polymers, which can respond to an electric field, the material offers sufficient mechanical strain by utilizing its electro-responsive deformation. In this actuator, the electroactive polymer was rolled-up with a center spring to support [17], [18]. The spring provides significant mechanical stiffness in the actuator, but its support stress is lack of adjustment. The advantage of electroactive materials simplifies the design of soft actuators considerably. However, due to the nonlinear electromechanical coupling process, the control algorithm of the actuation is very complicated, which can lead to various instabilities, including pull-in [19], snap-through [20], and wrinkles [21]. Sometimes, the electrical breakdown occurred, with a permanent failure under both the mechanical and electrical loading process [22]. Therefore, it is essential to find ways to combine the advantages of pneumatic and electric actuation, which should enable fast, stable, and reliable actuation.

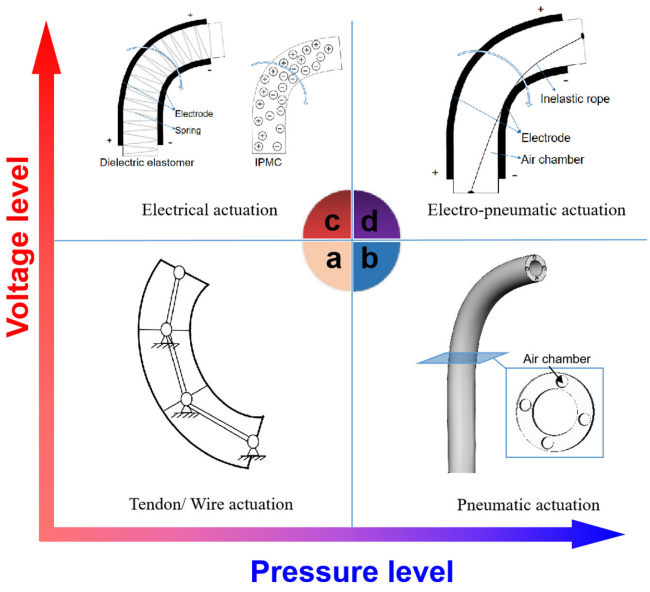

Fig. 1. Schematics of four types of actuation in soft robots. They are classified depending on whether they use or do not use voltage or pneumatic pressure. (a) Traditional tendon/ wire actuation method. (b) Pure pneumatic actuation with multiple air chambers. (c) Electric actuation methods in an electroactive polymer. (d) Novel electro-pneumatic actuation proposed in this article.

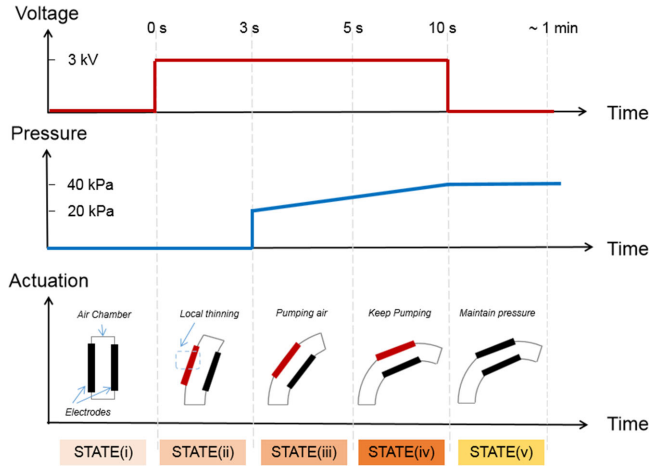

Fig. 2. Proposed control method for the soft bending actuator.

This study was designed to investigate a new actuation method that uses a dielectric elastomer with hybrid electro-pneumatic actuation. Dielectric elastomer is a type of electro-active polymer with strain over 100% [23]. This actuation behavior has been employed in developing new biomimetic soft robots [24]. In these soft robots, electrical excitation is the majority actuation strategy, while in this article, we propose a new approach. The approach includes a five-state control-method to enable a novel bending actuation, which exploits the local instability to increase the stroke range, realizing a combination of quick response and safe voltage operation. A single-chamber soft bending actuator [see Fig. 1(d)], which consists of a dielectric elastomer (DE), is used to combine the mechanical hyperelasticity and electroactive strain of DEs. The performance optimization and a simulation of the actuation were conducted to study the new actuation method. Besides, to demonstrate the advantages of this novel actuation approach, the performance of the single-chamber soft pneumatic actuators was compared to pure pneumatic actuators and pure electric actuators, followed by a detailed discussion.

II. Control Method for the New Soft Bending Actuator

An optimized control method was proposed to maximize the bending deformation of the soft hybrid actuator with precisely regulated low-voltage guidance. Based on our previous conclusion of the pneumatic actuator and electrical actuation in DE [25], we selected the voltage at 3 kV, pressure range as 20–40 kPa, and the timing as in Fig. 2. This enables rapid and significant stroke deformation with a soft DE actuator with low-voltage guidance to avoid both electrical breakdown and complicated structural design. It is possible to coordinate the electric-actuation and pneumatic actuation systematically via a timing sequence, which enables controllable actuation—see Fig. 2. By applying a low voltage to the actuator (shown in STATE i), a local thinning is induced at the stretching side, which causes slight bending in the direction opposite to the pull-in side (STATE ii). Subsequently, the pneumatic pressure is increased to drive the actuator (STATE iii) gently. When the pressure increased and exceeded a critical pressure, the actuator would bend rapidly (STATE iv), with an increased bending stroke. Finally, the actuator would maintain a large stable deformation after the voltage is removed on the DE membrane in STATE v. Surely, with more pairs of electrodes, the actuator can be guided to bending to more directions. We first characterize the one-direction bending and present the multidirection bending performance for demonstration. In this control strategy, the voltage is limited within 3 kV. Compared with conventional actuation voltage of DE that ranges from 6 to 20 kV, the 3 kV is relatively low and safe from electrical breakdown.

III. Experimental

A. Actuator Preparation and Actuation Experiments

To verify the concept shown in Fig. 2, we performed experiments. As shown in Fig. 3(a), a single-chamber actuator was prepared using the following six steps. The detailed description on manufacture is presented in the Methods Section.

After removing the preset steel-rod, the actuators were filled immediately with compressed air (20 kPa) to avoid rapid contraction along the height direction. The obtained actuators are displayed in Fig. 4. The actuation of the soft actuator mainly contains an electric actuation part and a pneumatic actuation part. As shown in Fig. 3(b), a signal generator (6811B Agilent TM) was used to output an electrical voltage signal, while a voltage amplifier (Model 610E TREK) was used to amplify the signal. As shown in Fig. 3(e), high-pressure gas was pumped using an air compressor. The pressure was modulated by a gas gauge (SMC IR1000-01). A dual signal was used to control the bending direction (guiding voltage). Furthermore, a larger-range stroke was facilitated by the pressure in Fig. 4. The bending

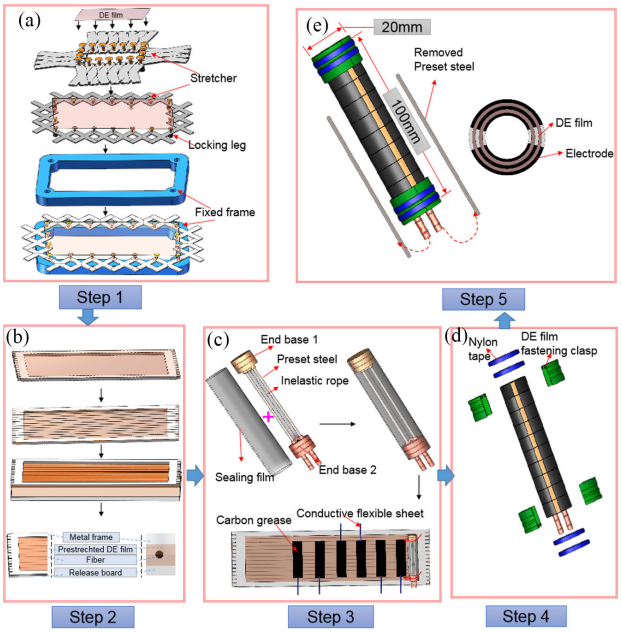

Fig. 3. Schematics of the actuator preparation and actuation experiments. (a) Prestretch of the DE-film (Step 1). (b) Combining the unidirectional fibers (Step 2). (c) Internal skeleton fabricating and electrode painting (Step 3). (d) Rolling the DE-film (Step 4). (e) Fastening the DE-film at the two end-bases (Step 5).

Fig. 4. Experimental characterization of the single-chamber bending actuator.

deformation was captured by the camera to measure the bending angle for further analysis.

B. Experimental Setup

The prestretch ratios of the DE-film can affect its electroactive response, and the bending performance of the electro-pneumatic actuator as well. To investigate the effects of the prestretch ratio, the prestretch values of A = 2.5, 3, and 3.5 were prescribed. To facilitate the induction of any bending direction in the actuator, a minimum voltage is needed for the DE actuator with different prestretch ratios, which is defined as critical voltage. The critical voltage was tested for each prestretch ratio, after which the actuators would bend at increasing angles with the increasing pressure. The angle measurement method is illustrated in Fig. 5.

To further investigate the effect of the size parameters on the actuation, the actuator was discretized into different flexible joints. This was done by placing a rigid disc inside the actuators [see Fig. 5(c)], and the prestretch ratio was fixed at 3. The effect of the ratio, the diameter D versus the height H, was explored for an unstable deformation induced by high pressure.

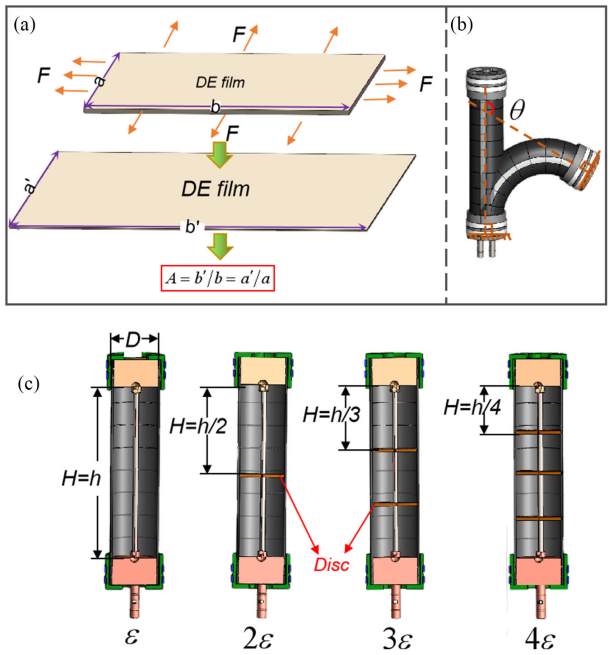

Fig. 5. Schematic showing the experiments. (a) Method of prestretch. (b) Method of measuring the bending angle. (c) Disc placement for the size parameter study.

C. FEM Simulation

Finite element analysis was conducted to simulate the actuation of the bending actuator. The finite element method (FEM) was implemented using the commercial software ABAQUS 6.14 and a user-subroutine (UMAT). The geometric model of the actuator, see Fig. 6, was built using the CAE module in ABAQUS. The solid linear hexahedron element was used to mash the part of DEs with hybrid integration (C3D8H). The end bases and hoop fibers were set as rigid bodies. The axial fiber part was a mesh with a 2-node linear 3-D truss element. The geometric parameters were set as follows: diameter (20 mm), hoop pre-stretch (3), electrode area: (170°), layer number (6), and fiber distance (5 mm). The detailed setting of the FEM is presented in the Methods Section.

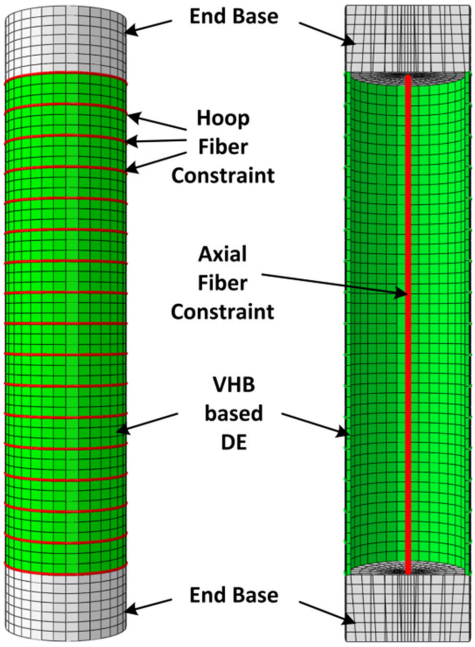

Fig. 6. Meshing and constraints used in the simulation.

IV. Results and Discussion

A. Effects of Prestretch of the DE-Films on the Critical Voltage

During the preparation of the soft bending actuator, the prestress of the DE-film makes it difficult for the actuator to be in a state of absolute homogeneity since the commercially available material is not consistent. Therefore, in the condition where no voltage is applied to counteract this deflection, as the air pressure in the internal cavity of the actuator increases, the actuator will bend toward an uncertain direction automatically. We define this automatic bending direction as the natural direction for its initialization—see Fig. 7(a). Therefore, to achieve effective induction of bending along another prescribed path, the applied voltage should at least be able to actuate the chamber to overcome the natural direction. In other words, it should succeed in guiding the actuators to bend toward by overcoming the natural inclination—see Fig. 7(b). Therefore, different voltages (from 2.0 to 5.0 kV) were applied in the actuators, with different prestretch ratios for bending-direction guidance. Under different voltages, both bending direction and bending angle were tested, as shown in Fig. 7(c), when the air pressure increased up to 40 kPa. It was found that the critical voltages are 5.0, 3.5, and 3.0 kV for the actuators with the prestretch ratios of 2.5, 3, and 3.5, respectively. The obtained critical voltages serve to calibrate the actuators in the desired bending direction.

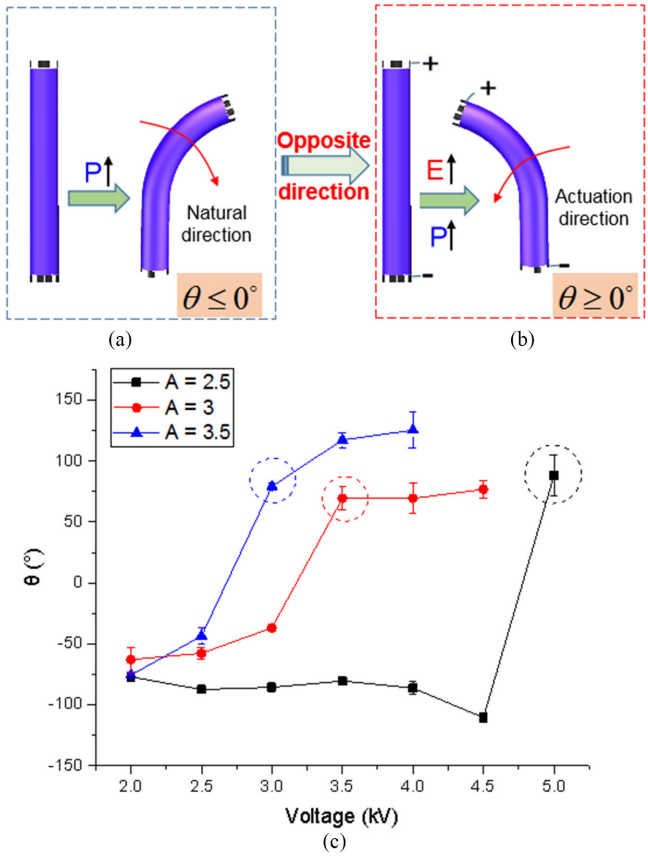

Fig. 7. Critical voltage of soft bending actuators with different prestretch ratios. Schematic diagram of (a) natural bending-direction and (b) actuation-direction opposite to the natural direction. *E* stands for the electrical voltage and *P* is the pneumatic pressure. (c) Results of the relationship between critical voltage and bending deformation.

B. Effects of Prestretch on the Bending Performance

In Section IV-A, it was verified that the DE actuators with different prestretch ratios have different critical voltages before bending direction guidance. In this section, the deformation of DE actuators with three different prestretch ratios was studied. After applying the critical voltage to the actuator for direction guidance, the pneumatic pressure was increased rapidly to obtain a large deformation. It can be seen from Fig. 8(a) that, as the pressure increases, three distinguishable stages can be noticed for the bending angle for the actuators with different prestretch ratios. At stage I, the bending angle gradually ramps toward a stable and maximum deformation. In stage II, the bending angle increases more rapidly in areas where sizeable bending strain begins to occur. In stage III, bending tends to be stable for a final maximum deformation angle.

Furthermore, it is observed that with the increasing prestretch ratio, the slope of the curve increased slightly during stages I and II, while the slope decreased slightly during stage III. As the prestretch ratio decreased, the maximum bending angle increased significantly. At the prestretch ratio of 2.5, the maximum bending angle exceeded 180°. Fig. 8(b) shows the snapshots of the bending process of the actuator with the prestretch ratio of 3 at different actuation stages, when the prestretch ratio was 3. The small bending angle, which was obtained in the process (1) to (2), mainly corresponds to the electric actuation for direction guidance with a constant voltage and low pressure at stage I. On the other hand, from (2) to (4), the rapid deformation due to the instability is shown in stage II. In stage III, the maximum bending angle is observed in (5).

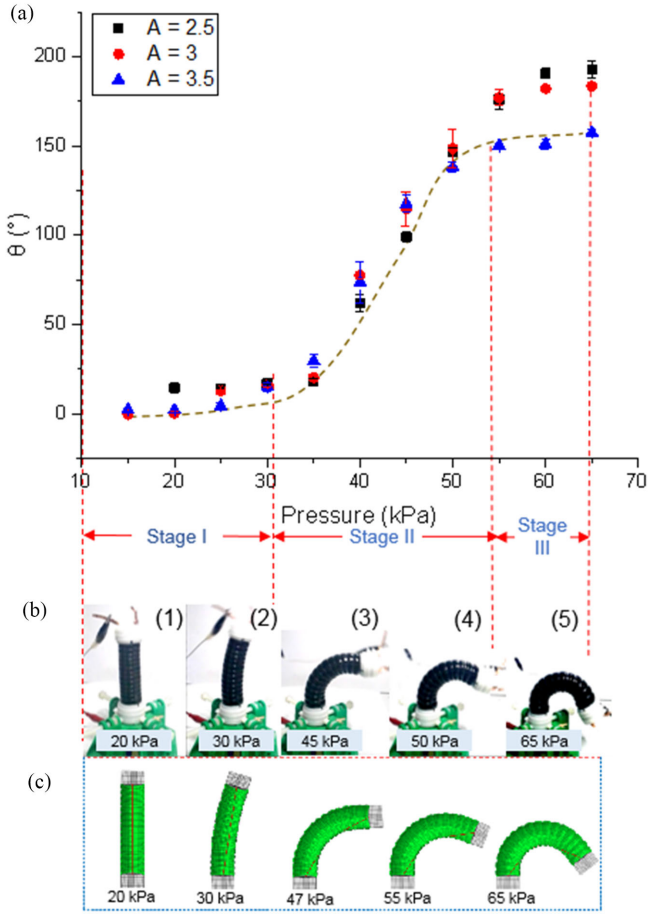

Fig. 8. Effect of air pressure on the bending angle. (a) Curves for soft bending actuators with different pre-stretch ratios; (b) and (c) represent, respectively, the real bending deformation figure and the simulation figure when different pressures are applied.

Moreover, in the simulation results, the complex contact process between axial fiber and DE is also shown. As illustrated in Fig. 8(c), when the pressure exceeds a specific limit, large and rapid bending actuation occurs, which is unstable concerning precise control for a targeted angle, and the axial fiber touches the DEs. Such a contact process may result in a high nonlinearity. The overall actuation method and deformation trend are consistent between the experimental results and the simulations.

C. Effect of Structural Parameters on the Actuation of Soft Bending Actuators

In addition to the prestretch ratios, structural parameters may also alter the actuation performance. As shown in Fig. 5(c), when different numbers of rigid discs are placed inside the actuator, the actuators can be divided into varying numbers of soft joints to form series-wound actuators. The bending angles, with pressure increase for D/H $= \varepsilon.,\varepsilon.,\varepsilon.,$and $4\varepsilon.,$are measured respectively. The results are shown in Fig. 9. The effect of D/H on bending performance is found more clearly at stage I and stage II, but trivial in stage III. At stage I, as D/H increases, the curve tends to be more flat, which indicates that the rise of D/H weakens the effect of the pressure on the deformation. During stage II,

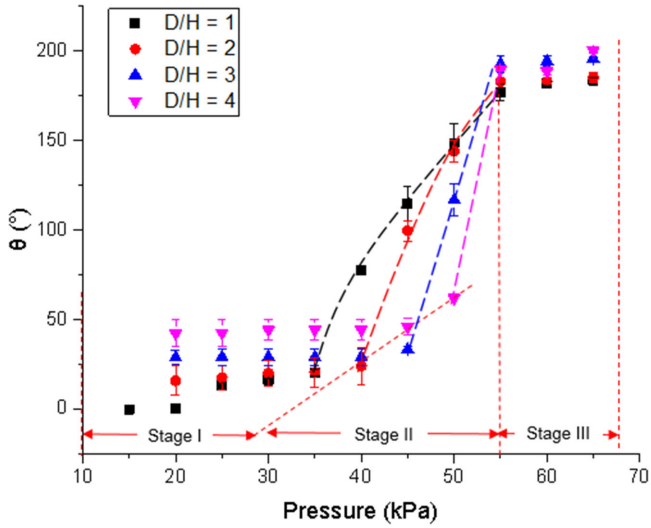

Fig. 9. Effect of the size parameter (D/H) on the bending angle.

the slope of the curve increases sequentially with increasing D/H. This means the low air pressure at stage I will amplify the deformation and instability in stage II. In stage III, where the stably maintained strain begins, both bending state and bending angle of all actuators overlap. This is due to the length of the string during the fabrication of the actuators. When the actuator is reaching the stage III, the length of the string limits its bending angle. Since the same string is employed, the final bending performance is almost identical.

V. Discussion

A. Performance Comparison With Three-Chamber Pneumatic Actuators

Chen *et al.* [26] reported a purely pneumatic actuator with three-chambers to achieve bending deformation in three directions. Their structural characteristics and general driving performance were compared with the single-chamber soft pneumatic actuator reported in this article (see Fig. 10). After applying the same pressure of 60 kPa to the two actuators, the single-chamber actuator reported in this article demonstrates a sizeable bending angle of 175.5, which is about six-fold more significant than the three-chamber counterpart of 25. Additionally, to achieve a bending angle of 100°, the single-chamber actuator only requires a pressure of 44.5 kPa. On the other hand, the pressure of the three-chamber actuator needs to be increased to about 140 kPa. This can be explained by the difference in the volume ratio for each driving-chamber for different actuators. As shown in Fig. 10, the volume of the driving chamber inside a single-chamber actuator exceeds 90%, while that of the three-chamber actuator is below 10%. Therefore, the tremendous driving load and small driving volume, which are caused by the complex structure, directly limit the driving potential of the three-chamber actuator. The blocking forces are different too. The three-chamber actuator has a thick-wall in its body, so it produced a higher force output. But the single-chamber actuator

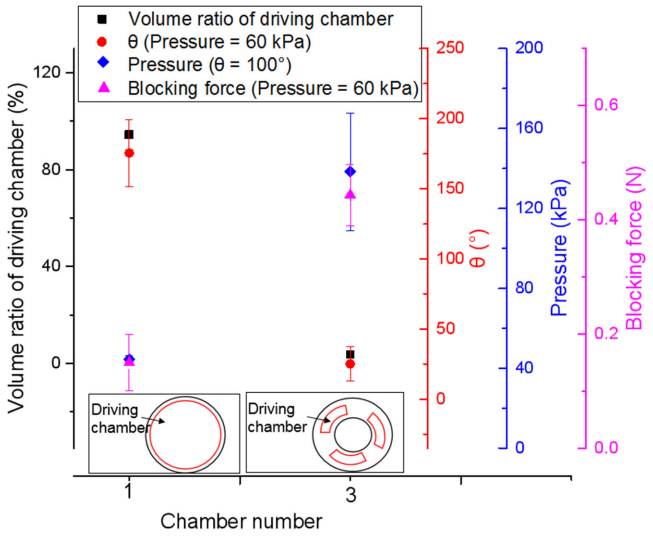

Fig. 10. Performance comparison between the single-chamber actuator and three-chamber actuator.

has thin wall thin which is prestretched, so the force is relatively small.

For the three-chamber actuator, each driving chamber is responsible for both direction-guidance and bending-actuation, which would finally lead to the complex structure and limited bending deformation. However, the single-chamber actuator uses the applied voltage to determine the bending direction. Moreover, it inflates to the only chamber to realize the large bending-deformation, which simplifies the structure and significantly improves the driving performance.

B. Performance-Comparison With Pure Electric Actuators

Fig. 11 shows the performance of the single-chamber pneumatic actuator and a pure electric actuator. As shown in Fig. 11(a), when the pressure in the chamber is constant, the actuation is only characterized by the electro-deformation property of the DE material. It is found that, although the bending deformation angle gradually increases with the increase of the voltage, the risk of breakdown also increases. When the voltage reaches 8 kV, the actuator can only be held at a deformation angle of 150° for about 1 s before the electrical breakdown of the actuators occurs.

As shown in Fig. 11(b), the bending direction is determined by applying a voltage of 3.5 kv, which produces thinning on one side of the actuator. Then, by increasing the air pressure in the chamber, rapid bending deformation in the prescribed bending direction is realized. The actuator, using this method, has the following advantages.

1) By increasing the pressure to more than 60 kPa, a large-angle deformation of about 180 ° can be achieved.
2) The characteristics of rapid aerodynamic strain are fully utilized.
3) The breakdown failure at high voltage is avoided.

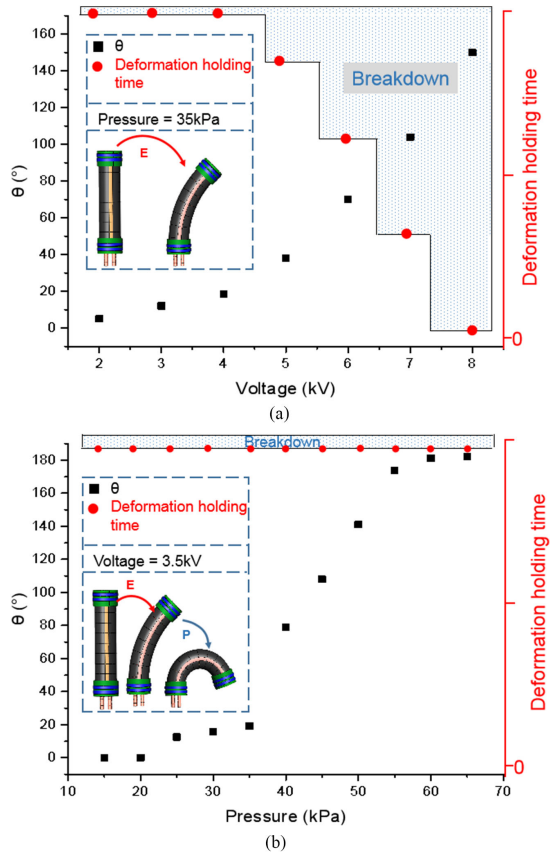

Fig. 11. Performance comparison between (a) the pure electric actuator and the (b) single-chamber pneumatic actuator.

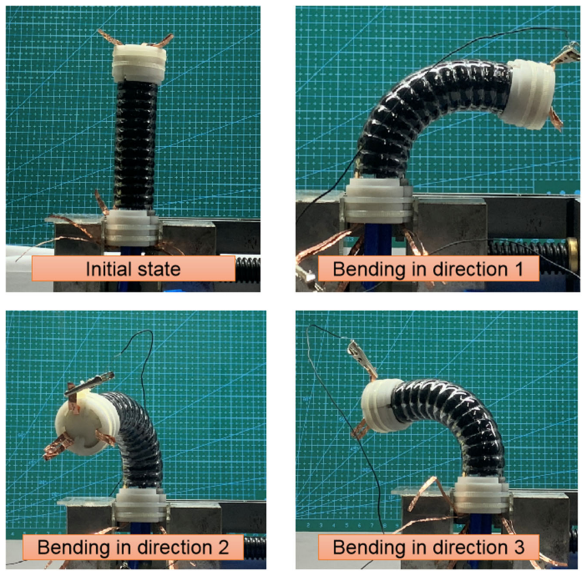

Fig. 12. Performance of multidirection bending.

C. Demonstration of Complex Bending Performance

To further demonstrate the bending performance, we present two examples. In Fig. 12, a single-chamber actuator with three-pairs of electrodes was fabricated. With pressure (20 kPa) in the whole chamber and voltage (3 kV) ON at any pair electrode,

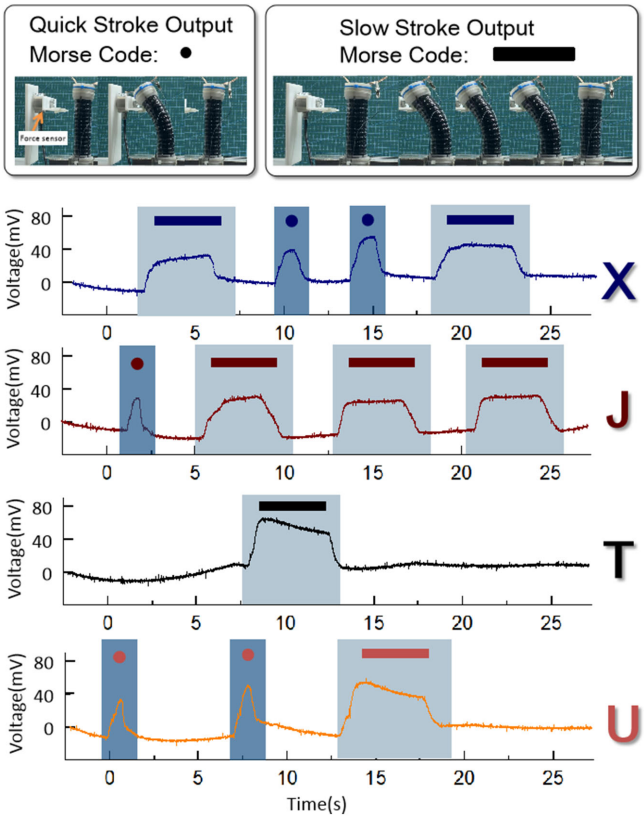

Fig. 13. Actuating the soft actuator to outputs Morse code as "XJTU."

where the local dielectric elastomer thinned local, the actuator bents in the opposite directions. The three-direction bending was realized, mimicking the three-chamber actuator.

We next demonstrate the application of the stroke. With voltage ON and OFF, the soft actuator is bending quickly and slowly, which can be used to programming the Morse Code. A force sensor measured the blocking force of the quick and slow bending, as shown in Fig. 13. With the proposed control method, the Morse Code of "XJTU" was generated and can be identified for a novel and safe human-machine to cognitive and interact.

VI. Conclusion

A single-chamber soft bending actuator was proposed in this article. It uses low-voltage direction guidance and high-pressure bending deformation, which successfully avoids the electrical breakdown failures of the pure electric actuators and the complex structure of the pure pneumatic actuators. The most significant bending angle of over 180 was obtained by the proposed actuator, which far exceeds the performance of the pure electric and pneumatic counterparts. Compared with a spring-supported roll-up actuator, the single-chamber actuator is pumped and sealed, its supporting stress is maintained and can be easily tuned through a gauge. The voltage in the actuation will surely promote the actuation response time and reduce the structural complexity if compared with pneumatics. But the leakage of the charge flow in the actuator may have a creep deformation in the muscle-like performance

The actuation process comprises three stages: the electric induction stage (Stage I), the unstable deformation stage (Stage II), and the stable large deformation stage (Stage III). The actuation process is consistent with the proposed control method. Based on a detailed analysis, it was found that the deformations at Stage I and Stage II are mostly affected by structural parameters such as the H/D ratio.

In contrast, the deformation at Stage III is strongly dependent on the prestretch ratio. As the prestretch ratio increased, the maximum bending angle decreased. Furthermore, as the H/D ratio increased, the change of the bending angle in Stage I reduces, while the deformation at Stage II accelerates. This study has also shown the control-ability and feasibility of the actuators, which opens new doors for industrial applications such as soft and continuous robots in the future.

Appendix

A. Method of Actuator Preparation

As shown in Fig. 3, a single-chamber actuator can be prepared using the following five steps:

1) The DE film is prestretched, equally in all directions along the plane as shown in Fig. 3(a). The DE film (VHB4905, 3M) is first stuck to the small cylinder on the stretcher. Then, the four locking legs on the stretcher are sequentially snapped into the four holes of the fixed frame to realize the prestretching of the DE film. The prestretched DE film is pasted on a metal frame and release board, respectively, for the next operation.
2) Anisotropic DE film is prepared as shown in Fig. 3(b). First, the fibers are tied to the teeth on both sides of the metal frame to make sure the distribution along the length of the metal frame. Then, the metal frame and the release board are bonded, where the fibers are sandwiched in the middle of the prestretched DE films to realize an in-plane anisotropic structure. The fiber is 0.128 mm diameter fishing line from DAYE Outdoor Company in China.
3) The internal sealing structure and external electrode distribution of the driver are shown in Fig. 3(c). First, the end base 1 and end base 2 are connected via an inelastic rope and two preset steels rod to form a core skeleton of the actuator. Then, the VHB4905 film without prestretching is used as the sealing film to wrap on the two end bases to form a closed single chamber inside of the actuators, where the inside of the DE film is painted with release agent (YINJING, U.S.) to prevent from sticking to the inelastic rope and the preset steels. Besides, carbon grease (supplied by the company MG) is evenly painted on the anisotropic DE film obtained in step (2) according to a predesigned template, and the electrode is drawn out using some conductive flexible sheets (Copper foil in the research) for voltage application. In the end, the DE film with carbon grease is rolled up around the core skeleton.
4) Four film-fastening clasps are placed at the end-bases then, and four Nylon tapes are tied around the film-fastening clasps to protect the DE film from detaching from the end bases as shown in Fig. 3(d).

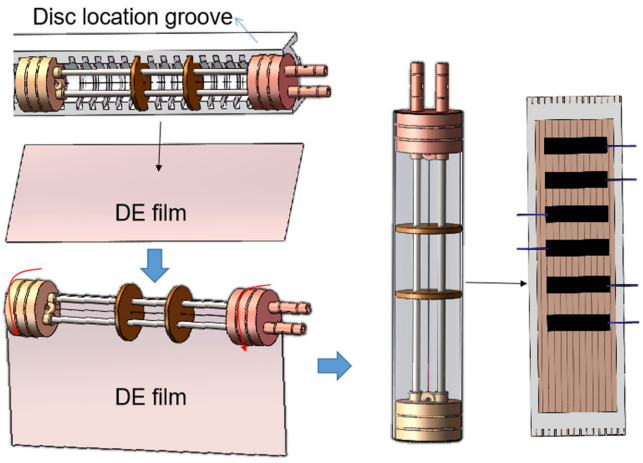

Fig. 14. Fabrication of the actuator with discs inside.

5) Finally, the actuator is successfully completed by removing the two preset steels through the holes at the end base 2, and the final electrode distribution are diagrammed as Fig. 3(e).

B. Method of Preparing Actuator With Discs

The difference between the preparation of the actuator with discs inside and without disc is mainly in the process of the internal skeleton with sealing film. As shown in Fig. 14, the discs and the two end bases should be placed in the disc locating groove in the appropriate positions of the card slot first. The preset steels and inelastic ropes are also used to connect the discs and end bases to form the internal skeleton. Then paste the internal skeleton to the DE film for sealing, where the DE film is not processed by the release agent to make sure the discs can be stably kept in the ideal position. Then, the expected internal structure can be formed by rolling the film. The subsequent process is the same as the method of preparing the actuator without discs.

C. FEM Simulation

In the simulations, we used finite element methods to establish the 3-D model for our actuators, as shown in Fig. 5, by the commercial nonlinear finite element package ABAQUS 6.14. In this process, the geometry parameters of the actuators were set as the same as the prototypes in the experiments, as follows: fiber interval is 5 mm, hoop prestretch is 3, electrode area is 180°, the diameter is 20 mm, layer number is 6. The 3-D models are meshed by using linear hexahedron element with hybrid integration (ABAQUS element type C3D8H) for both active and inactive regions, the basement and hoop fibers are set as a rigid body, and the middle fiber backbone has meshed with two nodes linear 3-D truss element. Moreover, the gravity of the actuators was also considered in this simulation. Under driving voltage, the electrical response of the DE material in the active region of actuators was captured by coding the free-energy function and its derivatives in a user-defined subroutine, UMAT. The Maxwell force was applied by defining a ground and a potential surface on opposite faces of the active region. In this configuration, the electrodes made of carbon grease are considered to have infinitesimal shear modulus, therefore to have a negligible mechanical contribution to the bending actuator, which is a reasonable assumption for grease type electrodes.

References

[1] M. T. Tolley *et al.*, "A resilient, untethered soft robot," *Soft Robot.*, vol. 1, no. 3, pp. 213–223, 2018.
[2] W. Hu, G. Z. Lum, M. Mastrangeli, and M. Sitti, "Small-scale soft-bodied robot with multimodal locomotion," *Nature*, vol. 554, no. 7690, pp. 81–85, 2018.
[3] T. Wang, J. Zhang, Y. Li, J. Hong, and M. Y. Wang, "Electrostatic layer jamming variable stiffness for soft robotics," *IEEE/ASME Trans. Mechatronics*, vol. 24, no. 2, pp. 424–433, Apr. 2019.
[4] M. Sitti, "Miniature soft robots—road to the clinic," *Nature Rev. Mater.*, vol. 3, no. 6, pp. 74–75, 2018.
[5] P. Hyatt, D. Kraus, V. Sherrod, L. Rupert, N. Day, and M. D. Killpack, "Configuration estimation for accurate position control of large-scale soft robots," *IEEE/ASME Trans. Mechatronics*, vol. 24, no. 1, pp. 88–99, Feb. 2019.
[6] G. Gu, J. Zou, R. Zhao, X. Zhao, and X. Zhu, "Soft wall-climbing robots," *Sci Robot.*, vol. 3, 2018, Art. no. 2874.
[7] T. Li *et al.*, "Fast-moving soft electronic fish," *Sci. Adv.*, vol. 3, no. 4, 2017, Art. no. e1602045.
[8] Y. Chen *et al.*, "Controlled flight of a microrobot powered by soft artificial muscles," *Nature*, vol. 575, no. 7782, pp. 324–329, 2019.
[9] C. Tang, W. Ma, B. Li, M. Jin, and H. Chen, "Cephalopod-inspired swimming robot using dielectric elastomer synthetic jet actuator," *Adv. Eng. Mater.*, vol. 22, pp. 1–10, 2020, Art. no. 1901130.
[10] R. V. Martinez *et al.*, "Robotic tentacles with three-dimensional mobility based on flexible elastomers," *Adv. Mater.*, vol. 25, no. 2, pp. 205–212, 2013.
[11] X. Dong *et al.*, "Development of a slender continuum robotic system for on-wing inspection/repair of gas turbine engines," *Robot. Comput.-Integr. Manuf.*, vol. 44, pp. 218–229, 2017.
[12] R. F. Shepherd *et al.*, "Multigait soft robot," *Proc. Nat. Acad. Sci.*, vol. 108, no. 51, pp. 20400–20403, 2011.
[13] C.-J. Cao, H. L. Hill, A. T. Conn, B. Li, and X. Gao, "Nonlinear dynamics of a magnetically coupled dielectric elastomer actuator," *Phys. Rev. Appl.*, vol. 12, no. 4, 2019, Art. no. 044033.
[14] F. Connolly, P. Polygerinos, C. J. Walsh, and K. Bertoldi, "Mechanical programming of soft actuators by varying fiber angle," *Soft Robot.*, vol. 2, no. 1, pp. 26–32, 2015.
[15] S. A. Morin, R. F. Shepherd, S. W. Kwok, A. A. Stokes, A. Nemiroski, and G. M. Whitesides, "Camouflage and display for soft machines," *Science*, vol. 337, no. 6096, pp. 828–832, 2012.
[16] B. Mosadegh *et al.*, "Pneumatic networks for soft robotics that actuate rapidly," *Adv. Functional Mater.*, vol. 24, no. 15, pp. 2163–2170, 2014.
[17] Q. Pei *et al.*, "Multifunctional electroelastomer rolls and their application for biomimetic walking robots," *Proc. SPIE*, vol. 4698, pp. 246–253, 2003.
[18] Q. Pei, M. Rosenthal, S. Stanford, H. Prahlad, and R. Pelrine, "Multiple-degrees-of-freedom electroelastomer roll actuators," *Smart Mater. Struct.*, vol. 13, no. 5, 2004, Art. no. N86.
[19] X. Zhao and P. Sharma, "Avoiding the pull-in instability of a dielectric elastomer film and the potential for increased actuation and energy harvesting," *Soft Mater.*, vol. 13, no. 26, pp. 4552–4558, 2017.
[20] B. Li, L. Liu, and Z. Suo, "Extension limit, polarization saturation, and snap-through instability of dielectric elastomers," *Int. J. Smart Nano Mat.*, vol. 2, no. 2, pp. 59–67, 2011.
[21] X. Liu, B. Li, H. Chen, S. Jia, and J. Zhou, "Voltage-induced wrinkling behavior of dielectric elastomer," *J. Appl. Polym. Sci.*, vol. 133, no. 14, pp. 1–8, 2016, Art. no. 43258.
[22] X. Liu *et al.*, "An electromechanical model for the estimation of breakdown voltage in stretchable dielectric elastomer," *IEEE Trans. Dielect. Elect. Insul.*, vol. 24, no. 5, pp. 3099–3112, Oct. 2017.
[23] A. O'Halloran, F. O'malley, and P. McHugh, "A review on dielectric elastomer actuators, technology, applications, and challenges," *J. Appl. Phys.*, vol. 104, no. 7, 2008, Art. no. 071101.

[24] G. Y. Gu, J. Zhu, L. M. Zhu, and X. Zhu, "A survey on dielectric elastomer actuators for soft robots," *Bioinspiration Biomimetics*, vol. 12, no. 1, 2017, Art. no. 011003.
[25] L. Liu, C. Zhang, M. Luo, X. Chen, D. Li, and H. Chen, "A biologically inspired artificial muscle based on fiber-reinforced and electropneumatic dielectric elastomers," *Smart Mater. Struct.*, vol. 26, no. 8. 2017, Art. no. 085018.
[26] Y. Chen, "Design, fabrication and performance of a flexible minimally invasive surgery manipulator integrated with soft actuation and variable stiffness," *J. Mech. Eng.*, vol. 54, no. 17, 2018, Art. no. 53.

Meng Luo received the B.S. degree in mechanical engineering and automation in 2014 from Xi'an Jiaotong University (XJTU), Xi'an, China, where he is currently working toward the Ph.D degree in mechanical engineering in the School of Mechanical Engineering.

His research interests include design and optimization of soft actuators and additive manufacturing of continuous fibers reinforced thermoplastic composites.

Lei Liu received the B.S. degree from the Xi'an University of Science and Technology, Xi'an, China, in 2009, the M.S. degree from Chang'an University, Xi'an, in 2011, and the Ph.D. degree from Xi'an Jiaotong University, Xi'an, in 2017, all in mechanical engineering.

He is currently a Lecturer with the School of Mechanical and Precision Instrument Engineering, Xi'an University of Technology. His research interests include electroactive smart materials, smart structures, and soft robotics.

Chen Liu received the B.S. degree in chemical engineering from Northwest University, Xi'an, China, in 2017, and the M.E. degree in mechanical engineering from Xi'an Jiaotong University, Xi'an, in 2020. He is currently working toward the Ph.D. degree in mechanical engineering with Queen Mary University of London, London, U.K.

His research interests include smart materials and structures, UAVs technique and vibration control technique.

Bo Li (Member, IEEE) received the B.Eng. degree in instrumental science and technology, from Southeast University, Nanjing, China, in 2006, and the Ph.D. degree in instrumental science and engineering from Xi'an Jiaotong University, Xi'an, China, in 2012.

He is currently an Associate Professor with the School of Mechanical Engineering, Xi'an Jiaotong University. His research interests include smart materials and soft robot.

Dr. Li is an Associate Editor of IEEE T-ASE.

Chongjing Cao received the B.Eng. degree in electrical and mechanical engineering from the University of Edinburgh, Edinburgh, U.K., in 2015, the B.Eng. degree in automotive engineering from the Dalian University of Technology, Dalian, China, in 2015, and the Ph.D. degree in robotics and autonomous systems from University of Bristol, Bristol, U.K., in 2019.

He is currently with the Shenzhen Institutes of Advanced Technology, Chinese Academy of Sciences, Shenzhen, China, where he is a Postdoc Researcher. His research interests include bioinspired robotic systems and dynamics of the smart materials.

Xing Gao was born in Zhuzhou, China. He received the B.E. degree in mechanical design, manufacturing, and automation from the Huazhong University of Science and Technology, Wuhan, China, in 2011, and the M.Sc. and Ph.D. degrees in mechanical engineering from Loughborough University, Loughborough, U.K., in 2012 and 2016, respectively.

He is currently an Associate Professor with the Research Centre for Medical Robotics and Minimally Invasive Surgical Devices, Shenzhen Institutes of Advanced Technology, Chinese Academy of Sciences, Shenzhen, China. In 2016 and 2018, he joined the Multi-scale Modelling and Simulation Laboratory, CNRS, France, and Bristol Robotics Laboratory, University of Bristol, U.K., as a Research Associate, respectively. His research interests include smart materials and soft robotics.

Dichen Li received the Ph.D. degree in material science and engineering from Xi'an Jiaotong University, Xi'an, China, in 1993.

He currently serves as the Changjiang Distinguished Professor and the Director of the State Key Lab for Manufacturing System Engineering, Xi'an Jiaotong University. He is also the Secretary-General for the branch of Additive Manufacturing (3-D printing) for Chinese Mechanical Engineering Society. His majors in additive manufacturing and biofabrication. He has published more than 400 papers and been granted more than 70 Chinese invention Patents.

Dr. Li was the recipient of a Second Prize of National Technological Innovation (China) and a Second Prize National Science and Technology Progress (China).